Flow Stress and Barreling Behavior of Aluminum Alloy Solid Cylinder during Upset Forging at Elevated Temperature

Thesis Submitted in Partial Fulfillment
of the Requirements for the Award of

Master of Technology
In
Production Engineering

By

Matruprasad Rout
Roll No: 209ME2203

Department of Mechanical Engineering
National Institute of Technology
Rourkela
2011

Flow Stress and Barreling Behavior of Aluminum Alloy Solid Cylinder during Upset Forging at Elevated Temperature

Thesis Submitted in Partial Fulfillment
of the Requirements for the Award of

Master of Technology
In
Production Engineering

By

Matruprasad Rout
Roll No: 209 ME 2203

Under the Guidance of

Prof. S.K. Sahoo

Department of Mechanical Engineering
National Institute of Technology
Rourkela
2011

ACKNOWLEDGEMENT

Successful completion of work will never be one man's task. It requires hard work in right direction. There are many who have helped to make my experience as a student a rewarding one.

In particular, I express my gratitude and deep regards to my thesis guide **Prof. S.K. Sahoo** first for his valuable guidance, constant encouragement and kind cooperation throughout period of work which has been instrumental in the success of thesis.

I also express my sincere gratitude to **Prof. R. K. Sahoo**, Head of the Department, Mechanical Engineering, for providing valuable departmental facilities.

I would like to give special thanks to Mr. L.N. Patra, PhD Scholar, Department of Mechanical Engineering, who gave his valuable time and support for this project work and without which the project might not be completed.

Last but not the least; I wish to express my sincere thanks to all those who directly or indirectly helped me at various stages of this work.

Matruprasad Rout

Roll No. 209 ME 2203

Dept. of Mechanical Engg.

National Institute Of Technology

Rourkela

CERTIFICATE

This is to certify that the thesis entitled, **"Flow Stress and Barreling Behavior of Aluminum Alloy Solid Cylinder during Upset Forging at Elevated Temperature"** submitted by **Shri Matruprasad Rout** in partial fulfillment of requirements for the award of Degree of Master of Technology in **Mechanical Engineering** with specialization in **"Production Engineering"** at National Institute of Technology, Rourkela, is an authentic work carried out by him under my guidance and supervision. To the best of my knowledge the matter embodied in the thesis has not been submitted to any other University or Institute for the award of any Degree or Diploma.

Date:

Dr. S.K Sahoo
Professor
Dept. of Mechanical Engg.
NIT, Rourkela

Abstract

Upset forging test at elevated temperature of aluminum alloy were experimentally carried out at specified temperatures ranging from 30°C (room temperature) to 300°C and at different true strain levels under a constant strain rate of 1 X 10^{-3}/s using powdered graphite mixed with machine oil as lubricant throughout the tests. Calculations were made to radius of curvature of barrel with the assumption that the curvature of the barrel followed the form of a circular arc. The radius of curvature of the barreled aluminum cylinders measured physically was found to confirm closely to the values calculated using the experimental data even at higher temperature. Generalized characteristic equations for each temperature have been developed by regression analysis. It was found that both the strength coefficient and strain hardening exponent decreases with increase in temperature. A common characteristic equation considering both strain and temperature was also found out. Further, different stresses like hoop stress, hydrostatic stress and effective stress have been found out for different temperature using the dimensions of the deformed specimens.

Keywords--Barreling, True Stress, True Strain, High Temperature, Regression Analysis

Nomenclature

d_0	Initial diameter of specimens
d_b	Barrel diameter of specimens
d_c	Contact diameter of specimens
h_0	Initial height of specimens
h_f	Final height of specimens
R	Radius of curvature of barrel
ε_z	Axial strain
ε_θ	Hoop strain
ε_e	Effective strain
σ_θ	Hoop stress
$\overline{\sigma}$	Effective stress
σ_m	Hydrostatic stress
σ_z	Axial stress
α	Slope between hoop strain and axial strain
SSE	Sum of Squares for Error
RSME	Root Mean Square Error
R^2	Regression Square

List of Figures

Chapter 1

Chapter 3

Chapter 4

List of Tables

Chapter 2

Chapter 3

Chapter 4

Contents

Chapter 1
Introduction

1. Introduction

1.1 Upset Forging

Many operations in manufacturing, particularly processes such as forging, rolling, and extrusion are performed with the workpiece subjected to compressive forces. The compression test, in which the specimen is subjected to a compressive load, gives information useful for these processes. The test is usually carried out by compressing a solid cylindrical specimen between two flat dies. Because of friction between the specimen and the dies, the specimen's cylindrical shape bulges, this effect is called barreling. Friction prevents the top and bottom surfaces of the specimen from expanding freely.

Because the cross-sectional area of the specimen now changes along its height, being maximum in the middle, obtaining stress strain curves in compression is difficult. Furthermore, friction dissipates energy, so the compressive is higher than it otherwise would be, in order to supply the work to overcome friction. With effective lubrication, friction can be minimized, and a reasonably constant cross-sectional area can be maintained during the test.

Upset forging or simple axial compression testing is useful for measurement of elastic and compressive fracture properties of both ductile and brittle materials. The true stress-true strain curves obtained from the compression test and tension tests on ductile materials coincide with each other, where as this does not hold true for brittle materials, which are generally stronger and more ductile in compression than in tension.

1.2 Modes of Deformation

The shape of the specimen after compression largely depends on the aspect ratio (*h/d*) of the specimen. Figure 1.1 shows the modes of deformation in compression testing. (a) Buckling, when $h/d > 5$. (b) Shearing, when $h/d > 2.5$. (c) Double barreling, when $h/d > 2.0$ and friction is present at the contact surfaces. (d) Barreling, when $h/d < 2.0$ and friction is present at the contact surfaces. (e) Homogenous compression, when $h/d < 2.0$ and no friction is present at the contact surfaces. (f) Compressive instability due to work-softening material.

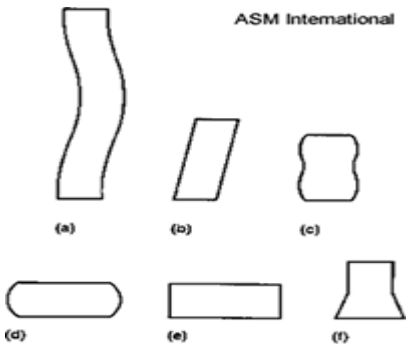

Figure 1. 1 Modes of Deformation

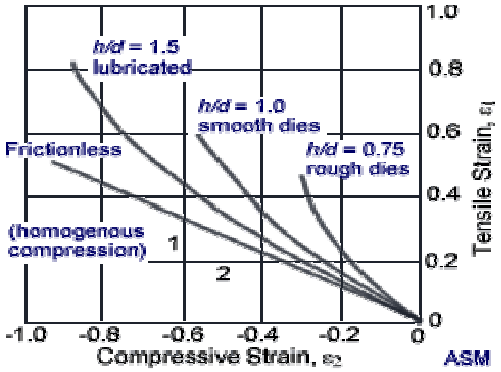

Figure 1. 2 Variation of Strain

In any case, the use of specimens having large *h/d* ratios should be avoided to prevent buckling and shearing modes of deformation.

Figure 1.2 shows variation of the strains during a compression test and tensile test without friction (homogenous compression) and with progressively higher levels of friction and decreasing aspect ratio *h/d*.

1.3 Upset Forging at High Temperature

1.3.1 Effects of Temperature

Increasing temperature generally has the following effects on stress strain curves:

a. It raises ductility and toughness, and

b. It lowers the yield stress and modulus of elasticity

Temperature also affects the strain hardening exponent of most metals, in that n decrease with increasing temperature. The influence of temperature is however best described in conjunction with the rate of deformation.

1.3.2 Effects of Rate of Deformation

The rate at which strain is applied to a specimen can have an important influence on the flow stress. Strain rate is defined as: $\dot{\varepsilon} = d\varepsilon/dt$, and is conventionally expressed in units of s^{-1} i.e. per second. Generally, increasing strain rate increases flow stress. Moreover, the strain rate dependence of strength increases with increasing temperature.

The true strain rate is given by

$$\frac{d\varepsilon}{dt} = \frac{d[ln(h/h_o)]}{dt} = \frac{1}{h}\frac{dh}{dt} = \frac{v}{h} \qquad (1)$$

Where *v* is the crosshead velocity

The above equation indicates for a constant crosshead speed the true strain rate will increase as the specimen length decreases. So in order to make true strain rate constant, crosshead velocity should be decrease with decrease in specimen height.

1.4 Aluminum alloy:

Aluminum alloys are alloys in which aluminum (Al) is the predominant metal. Commercial purity of aluminum is 99.5 to 99.79%, but pure aluminum is too soft to be of structural value. The primary reason for alloying aluminum is to increase strength without significantly increasing weight. Other reasons are to improve machinability, weldability, surface appearance and corrosion resistance. The typical alloying elements are copper, magnesium, manganese, silicon, and zinc.

1.4.1 Alloy designation:

Wrought and cast aluminum alloys use different identification systems. Wrought aluminum is identified with a four digit number which identifies the alloying elements where the first digit indicates the major alloying elements.

Cast aluminum alloys use a four to five digit number with a decimal point. The digit in the hundreds place indicates the alloying elements, while the digit after the decimal point indicates the form i.e. cast shape or ingot.

1.4.2 Applications:

Aluminum alloy has wide range of application. Followings are some of them.

I. In aircraft and other aerospace structures
II. for boat and shipbuilding, and other marine and salt-water sensitive shore applications
III. for cycling frames and components
IV. for automotive body panels
V. As a packaging materials.
VI. In making household components etc.

Chapter 2
Literature Reviews

2. Literature Reviews

Due to the huge application of metal forming in the field of manufacturing, many investigators have carried out a series of investigations on upset forging at cold stage as well as at hot stage of different materials. Many investigators has carried out the experiment at high temperature by taking temperature and strain rate as main effecting parameters and found out the flow behavior and microstructure evaluation of material. Some of the investigators have predicted the flow stress of the material by using some algorithms such as fuzzy logic, neural network, genetic algorithm etc. Followings are some literature review which is carried out during this project work.

2.1 On hot upset forging:

- Jin Nengping. et.al. [1], showed that, the peak stress level of 7150 aluminum alloy decreases with increasing deformation temperature and decreasing strain rate. The deformed structures exhibit elongated grains with serrations developed in the grain boundaries Dynamic recovery and recrystalization are the main reasons for the flow softening at low Z value..
- Poursina. M. et.al. [2], found out that, in hot deformation of stainless steel work hardening can be neglected and constitutive equation can be taken as a function of strain rates only. The suggested constitutive equation was also reconfirmed by comparing the geometrical deformation of the specimens and numerical simulation of the compression test.
- Zhang Hui et.al. [3], found out that, the true stress strain curves of Al-Mg-Si-Cu aluminum alloy exhibit a peak stress at a small strain, after which flow stress decrease monotonically until high strain. The substructure in the deformed specimens consists of

very small amount and fine precipitates with equaxied polygonized subgrains in the elongated grains and developed serrations in the grain boundaries.

- Xiu-yu WEI. et.al. [4], concluded that, the flow stress of 2197 Al-Li alloy decreases with the increase of deformation temperature and increases with the increase of strain rate. The peak flow stress during high temperature deformation can be represented by *Z* parameter in a hyperbolic sine function.
- Cerri.E. et.al. [5], found out that, the stress–strain curves of AZ91 magnesium alloy can be explained in terms of microstructure evolution, with emphasis on the eutectic phase and on dynamic precipitation phenomena occurring at low and high temperature of deformation.
- Zhu. Su-Ming. et.al. [6], found out that, the Fe-25Al alloy can be deformed without cracking at temperatures above 873 K. The results show that Ti addition tend to reduce the strain rate sensitivity and activation energy for flow deformation of Fe-25Al alloy.
- Zhang.X.Y. et.al. [7], showed that, the apparent activation energy for deformation of TC11 titanium alloy increases with the increasing of deformation temperature gradually, and decrease with the increasing of strain rate.
- Herrmann. J. et.al. [8], found out that, heat treatments of Fe-Al alloys at temperatures below 600°C, has no major impact on the deformation behavior. Only heat treatments at temperatures above 600°C affect the mechanical behavior significantly.
- Talebi Ankari. M. et.al. [9], uses ANN and inverse method to predict the flow stress for AZ61 Mg- alloy. The predicted results depicted a good agreement with the experimental data even if the ANN results shown the best predicted capability.

- Mousavi Anijadan. S.H. et.al. [10], taken ANN and genetic algorithm to optimize the flow stress of 304 stainless steel under cold and warm compression. The combined algorithm offers an effective condition for the material, which avoids flow localization, dynamic strain aging, adiabatic shear deformation and void generation.
- Aluko O. et.al. [11], found out that the compression curves of aluminum alloy obtained using the barrel correction factor method and the Bridgman re-machining technique (no barreling allowed during the test) are found to have close values, even at higher temperatures. The true-stress versus true-strain curves and the barrel sizes obtained follow empirical power laws, even at higher test temperatures.
- Mandal S. et.al. [12], developed a Constitutive equation considering compensation of strain and strain rate of alloy D9. The new constitutive equation break downs at the processing conditions due to the adiabatic temperature rise during high strain rate deformations. Chen. Z.Y. et.al. [13], has taken Hill's general method to calculate the flow stress of a cylindrical specimen of AA6063 aluminum alloy under uniaxial simple compression and also to consider the friction effect at the die-specimen interface. Both the results of FEM analysis and compression test were combined to evaluate the friction coefficient.
- Ramanathan. S. et.al [14], found out the optimum working regions and flow instable regions of 2124 Al alloy manufactured by powder metallurgy method, by using processing maps. They also found the power dissipation efficiency and instability parameters of the material.

2.2 On cold upset forging:

- A no. of investigation has been carried out by Narayansamy. R, et.al. [15-18] on cold upset forming of different materials of different shape. A new geometrical shape factor (GSF) has been established based on the dimensions of the deformed specimens. It was found by them, that the measured barrel radius of curvature follows a straight line relationship with the GSF. Empirical relationship was also made for finding out different stresses acting on the specimen during upset forming like hoop stress, hydrostatic stress and effective stress.
- Manisekar K, et.al. [19], studied on the effect of friction during the cold upset forming by taking different frictional conditions and concluded that bulging produced is the lowest for molybdenum disulphide irrespective of the aspect ratio.
- Malayappan S. et.al. [20], also made analysis on effect of friction and concluded that the final shape of the work-piece after the upsetting process can be divided into two geometries namely a barreled portion and a truncated cone portion and the new hoop strain slope is found to increase accordingly with increasing aspect ratio.
- Sljapic. V. et.al. [21], studied on fracture in axi-symmetric and three dimensional cold upsetting of brass and concluded that the material exhibit a transition from ductile to brittle behavior under the room temperature, quasi-static test conditions.

To reduce the role of friction on the test result proper lubricant should be used. Followings are some lubricants used by different investigators for different material at high temperature.

Table 2. 1 Lubricants used at high temperature by different investigators for different material

Investigators	**Workpiece Material**	**Temperature range**	**Lubricants used**
Zhang Hui. et.al.	Al-Zn-Mg-Cu-Zr alloy	300-450°C	Graphite mixed with machine oil
Talebi Ankari. M. et.al	AZ61 Mg alloy	250-350°C	Graphite
Jin Nengping. et.al	7150 Al alloy	300-450°C	Graphite mixed with machine oil
Mandal s. et. al	Alloy D9	850-1250°C	Borosilicate glass paste
Zhang Hui. et.al.	Al-Mg-Si-Cu aluminum alloy	350-550°C	Graphite mixed with machine oil

Some other lubricants which are used at high temperature are molybdenum disulfide grease-base, Teflon sheet, Molycote spray, carbon foil and so on.

Chapter 3
Experimental Details

3. Experimental Details

3.1 Experimental Setup

The experiments were carried out in the universal testing machining of INSTRON SATEC KN 600. KN Models of INSTRON are ideal for high capacity tension, compression, flex and shear testing. These models feature an ultra large, single test space and so users can easily and safely load and unload specimens. This design offers the ultimate in versatility by accommodating a large variety of specimen sizes, grips, fixtures and extensometers. Models include: 300KN, and 600KN, 1200KN, 1500KN, 2000KN and 3500KN.

3.1.1 INSTRON SATEC KN 600 Specifications

Followings are the specifications of the machine

Table 3. 1 Specifications of INSTRON SATEC KN 600

Maker	INSTRON
Model	SATEC KN 600
Maximum Capacity	600 KN
Design Capacity	480 KN
Horizontal Test Width	711 mm
Horizontal Test Depth	762 mm
Stroke	508 mm
No. of Columns	2
Testing Speed Range (at full load)	0.1 to 203 mm/min
Jog Adjusting Speed (max.)	203 mm/min

3.1.2 Furnace

These three zone resistance wire wound furnaces are of split construction to facilitate fast and easy loading of a pre-assembled specimen train. The case is constructed from stainless steel with aluminum and hardened insulation board end plates. The optional front cut-out allows the use of side-entry high-temperature extensometry. Adjustable stainless steel latches keep the furnace halves locked together during use, but are then easily opened once testing is complete. The furnace is available with optional heavy duty brackets or mountings, which attach to a wide range of testing systems. The resistance wire is wound on to recrystallized alumina tube in three independent zones to form the furnace element. This three-zone format allows the user to tailor the furnace temperature gradient, creating a uniform central zone. High-performance ceramic fiber insulation is used to reduce heat losses and provide fast heating rates.

3.1.3 Furnace Specifications

Table 3. 2 Specifications of Furnace

Model and Style	SF- 16, 2230
Heat Zone Length	280 mm
No. of Zones	3
Element Resistance per Zone	17.6 Ohms
Furnace Length	330 mm
Furnace Outside Dia.	255 mm
Internal Bore Dia.	75 mm
Weight	21 Kg. (approx.)
Operating Temperature	1200°C
No. of Thermocouples	3

Thermocouples Type	K
Power Requirement	
Voltage	115 Vac.
Watt	2250 W, 750 W/ Zone
Phase	Single
Ampere	21 A, 6.52A/ Zone
Hertz	60 Hz/ 50 Hz
Temperature Controller Type	Eurotherm 2416
No. of Controller	3

3.1.4 Hydraulic Power Supply

Table 3. 3 Hydraulic Power Supply

Model	V22a
Height	1030 mm
Required Floor Space	(1220×935) mm
Weight	522 Kg. (approx.)
Required Flow at Maximum Testing Speed	12.37 Lpm
Ideal Pressure	28 bar
System Relief Pressure	179 bar
Motor Power	5 hp

Figure 3. 1 Furnace

Figure 3. 2 Temperature controller

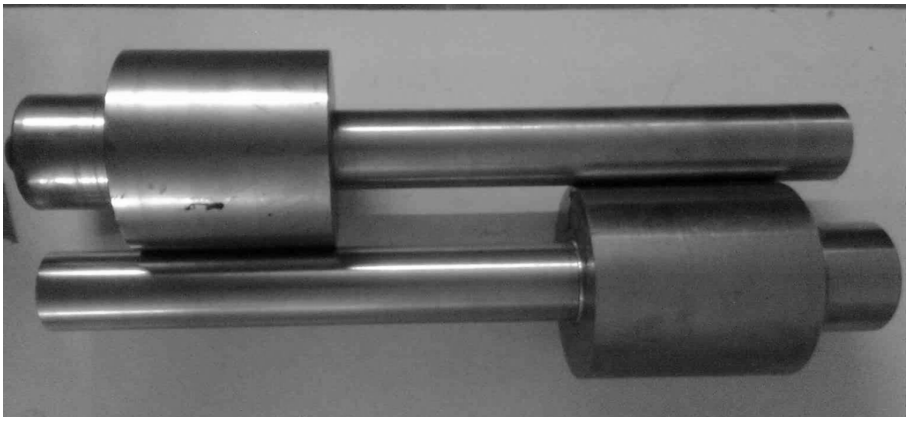

Figure 3. 3 Experimental set up for high temperature compression test

Figure 3. 4 INSTRON with set up for high temperature compression test

3.2 Graphite as a lubricant:

Graphite is one of the allotropes of carbon. It is structurally composed of planes of polycyclic carbon atoms that are hexagonal in orientation. The distance of carbon atoms between planes is longer and therefore the bonding is weaker. Graphite is best suited for lubrication in a regular atmosphere. In an oxidative atmosphere graphite is effective at high temperatures up to 450ºC continuously and can withstand much higher temperature peaks. Graphite is characterized by two main groups, natural and synthetic. Graphite as a lubricant is used as dry powder or mixed with water or oil. When mixed with water, it is called 'aqua-dag' and when mixed with oil,

it is called 'oil dag'. Graphite powder and machine oil in a proper ratio were mixed properly to form the lubricant for the test.

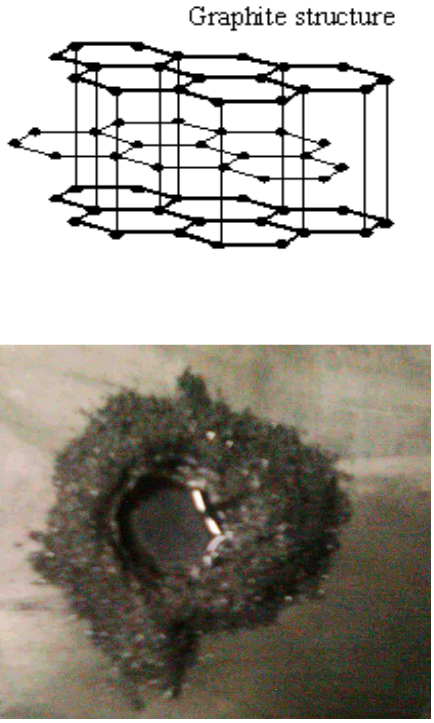

Figure 3. 5 Mixing of graphite powder with machine oil

3.3 Procedure

The total experimental work can be divided into two parts,

1. Specimen preparation
2. High temperature compression test in INSTRON

3.3.1 Specimen Preparation

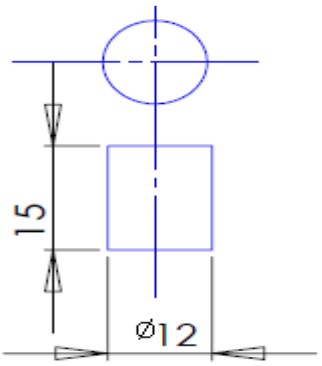

Figure 3. 6 Specimen Dimensions

The aluminum alloy which was used for this project work has the following composition.

Table 3. 4 Composition of the Specimen

Element	Al	Si	Mg	C	O
Weight %	83.68	0.28	0.78	13.71	1.54

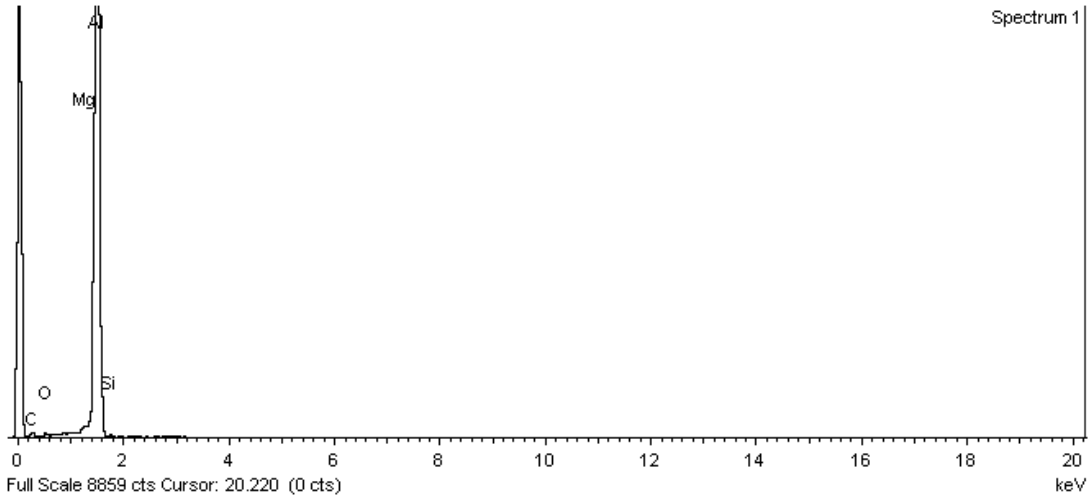

Figure 3.7 Material Composition

Specimens of the required dimensions (figure 3.6) were cut from the aluminum alloy bar and facing operation is carried out to make the two ends parallel. Two no. of small holes of 1 mm (approx.) depth were drilled at both the ends to accumulate the lubricants.

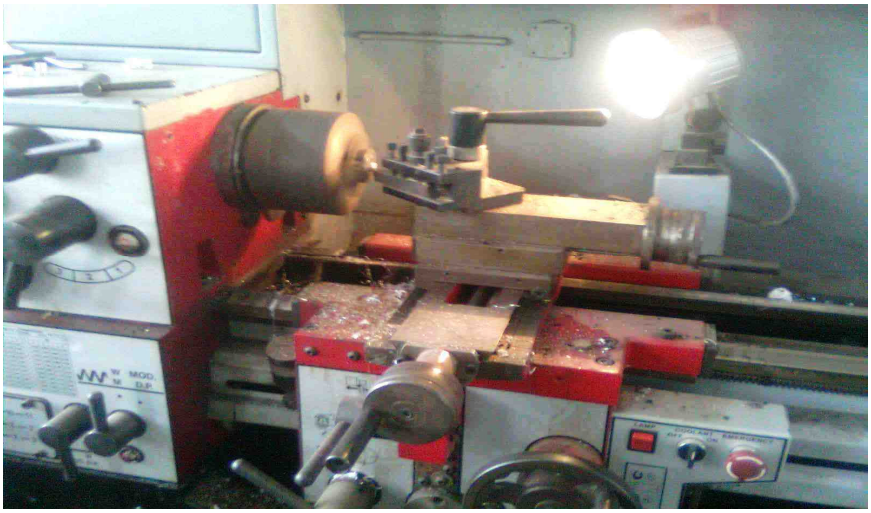

Figure 3. 8 LATHE Machine

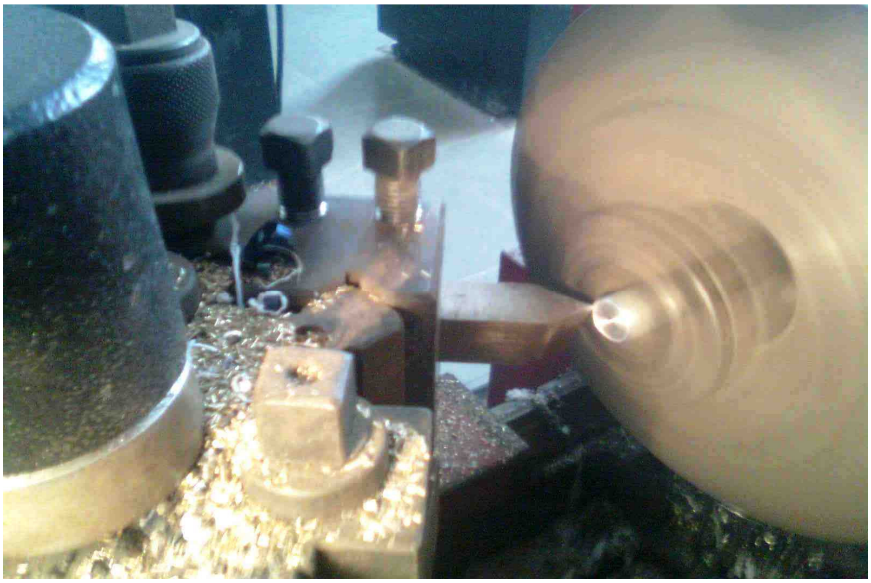

Figure 3. 9 Specimen Preparations on LATHE

Figure 3. 10 Specimens

3.3.2 High temperature compression test in INSTRON

Specimens with lubricant coating on both the end are placed in between the top and bottom platen of the setup. Extreme care was taken to place the axis of the cylindrical specimen concentric with the axis of the ram. Furnace is now closed and the specimen is heated up to the desired temperature at a rate of 6°C / min approximately. Specimens are held on the testing temperature for 2-3 min after achieving the desired temperature for uniform heating. Then hydraulic load is applied for the testing. The test is carried out at constant temperature. For each temperature test, six specimens of the same dimensions were taken and deformed to different strain levels. The loads used during each deformation were recorded automatically by the BLUEHILL software incorporated with the UTM machine. Compressive test was carried out maximum up to a true height strain of 1 and at temperature of 30°C, 100°C, 150°C, 200°C, 250°C and 300°C. After each test, the following parameters were measured: (i) the height of the deformed specimen (h_f); (ii) the contact diameter of the specimen (d_c); (iii) the bulged diameter (d_b); and (iv) radius of the barrel (R). The barrel radius at each deformation was measured using CALIPER PRO software incorporated with an optical microscope and the rest of the dimensions were measured by digital vernier caliper.

Figure 3. 11 Specimen within the furnace

3.4 Specifications of Optical Microscope

Table 3. 5 Specifications of Optical Microscope

Maker	Radical Instrument
Model	OM-19
Camera	Digital CCD Colour Camera
Zoom Magnification	7X to 45X
X-Y Measuring Stage	150×150 mm
Digital Readout System L.C	0.001 mm
Fluorescent Ring Illuminator	

Figure 3. 12 Optical Microscope

Figure 3. 13 Digital Vernier Caliper

Chapter 4
Results and Discussions

4. Result and Discussions

4.1 Flow Curve

A true stress-strain curve is frequently called a flow curve because it gives the stress required to cause the metal to flow plastically to any given strain. Many attempts have been made to fit mathematical equations to this curve. The most common is a power expression of the form

$$\sigma = K\varepsilon^n \tag{2}$$

Where K is strength coefficient or stress at ε= 1.0 and n is the strain hardening coefficient.

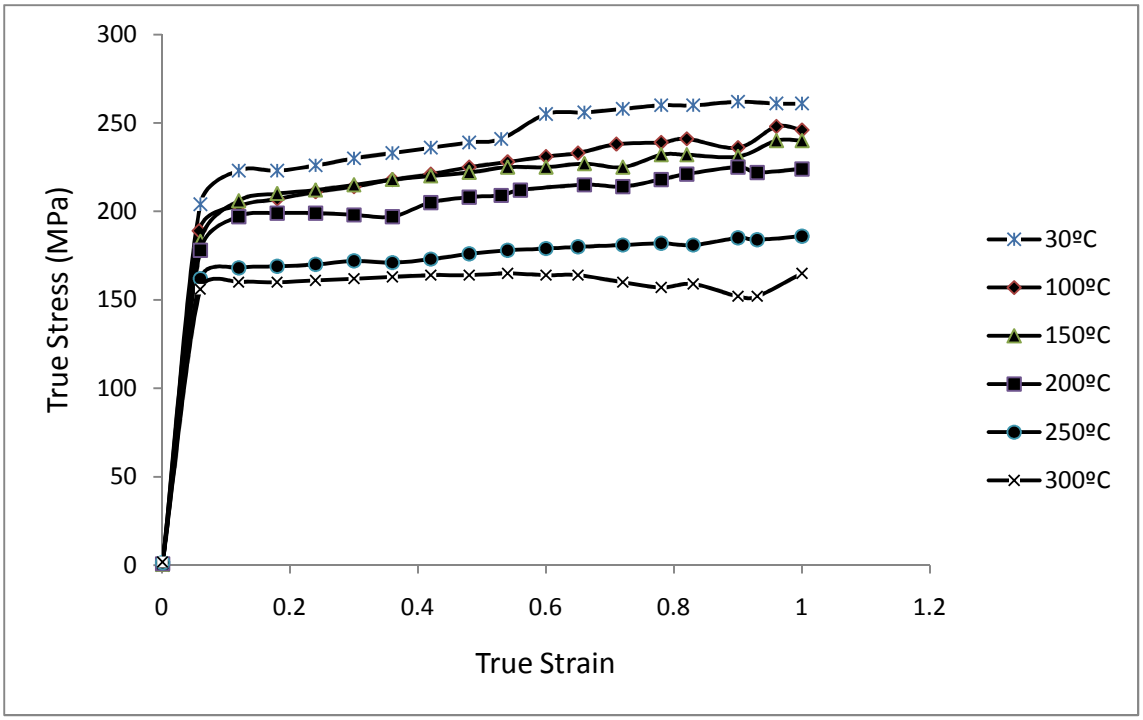

Figure 4. 1 True Stresses vs. True Strain Curve for Different Temperature

Figure 4.1 shows the flow curve of the material at different temperature. Data taken in regular interval during the experiment by the BLUEHILL software were taken to plot the flow curve. It was clear from the graph that the flow stress decreases with the increase in temperature, as the material get soften with the increase in temperature or flow-ability of the material increases.

(a) Temperature 30°C

(b) Temperature 100°C

(c) Temperature 150°C

(d) Temperature 200°C

(e) Temperature 250°C

(f) Temperature 300°C

Figure 4. 2 Deformed Specimens at Different Temperature

4.2 Non linear least square regression analysis

Regression analysis may be defined as the technique for modeling and analyzing variables, to make a relationship between a dependent variable and one or more independent variables. It helps one to understand how the value of the dependent variable changes when any one of the independent variables is varied, while the other independent variables are held fixed. A large no of techniques have been developed for carrying out regression analysis. Out of all those, linear regression and least squares regression are more commonly used. Least squares problems fall into two categories: linear least squares and non-linear least squares, depending on the nature of variation of the dependent variable with the independent variables. The main difference between these two is linear least square has a closed-form solution where as the non-linear has no closed-form solution and is usually solved by iterative refinement; at each iteration the system is approximated by a linear one. Followings are the results obtained by non linear regression analysis using MATLAB software:

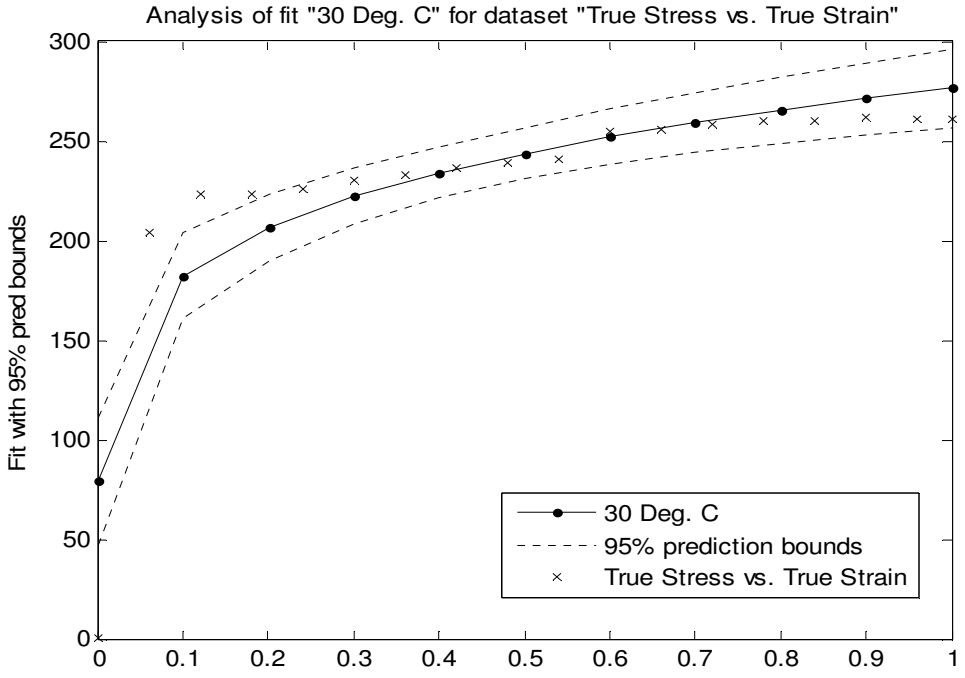

(a) Coefficients: $k = 276.5, n = 0.1814$

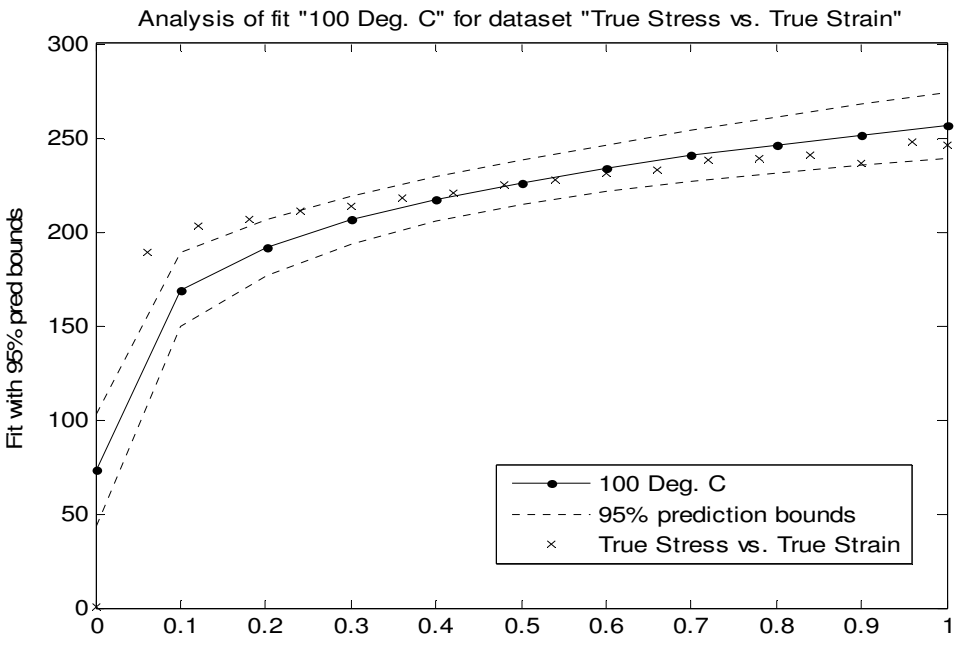

(b) Coefficients: $k = 256.4$, $n = 0.1817$

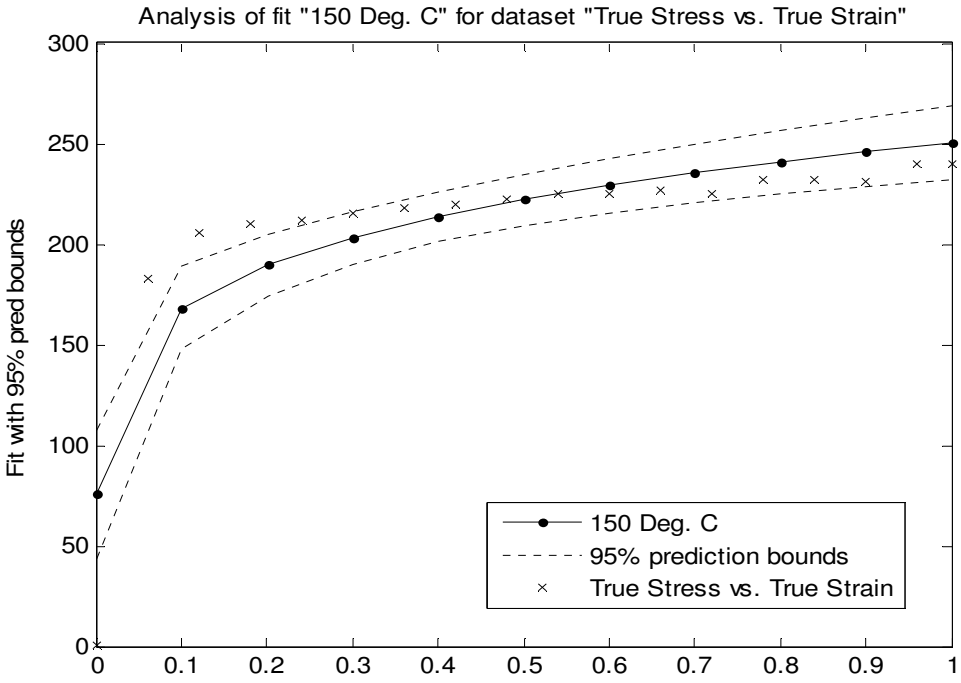

(c) Coefficients: $k = 250.2$, $n = 0.173$

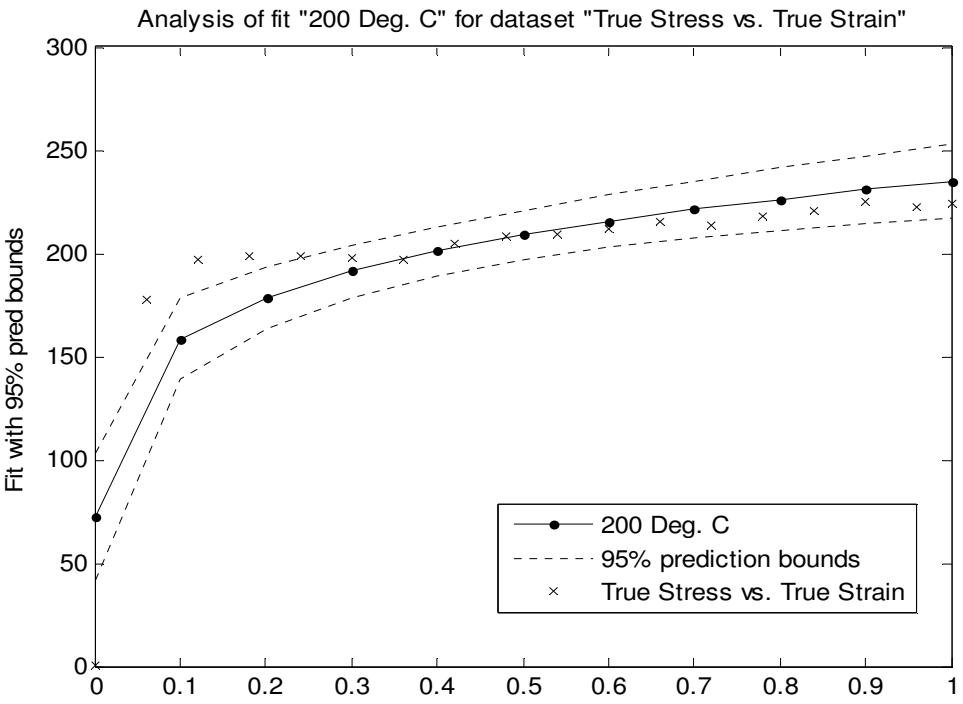

(d) Coefficients: $k = 235.1$, $n = 0.1712$

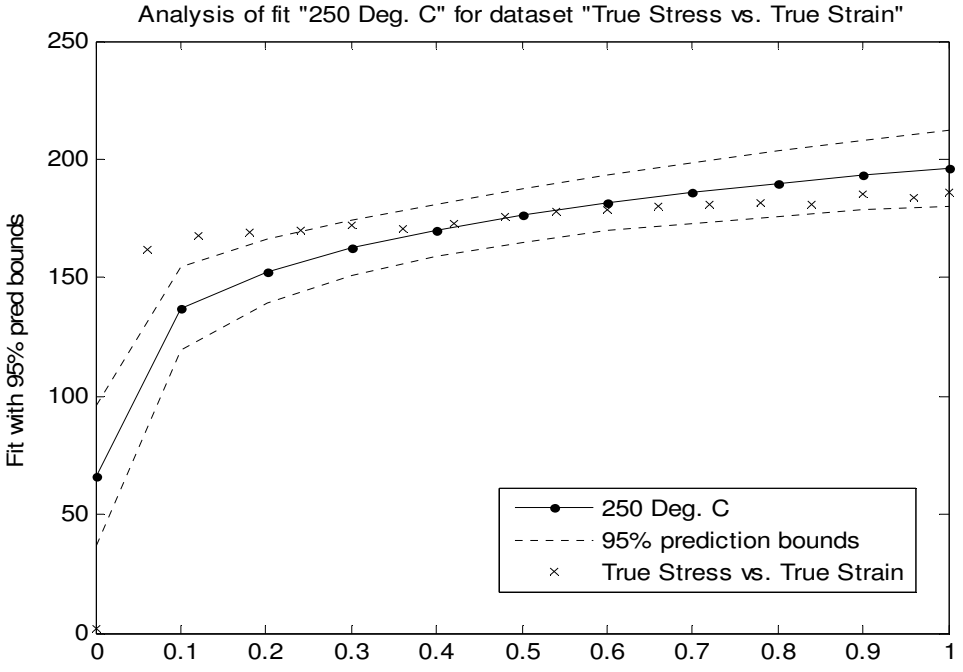

(e) Coefficients: $k = 196.6$, $n = 0.1575$

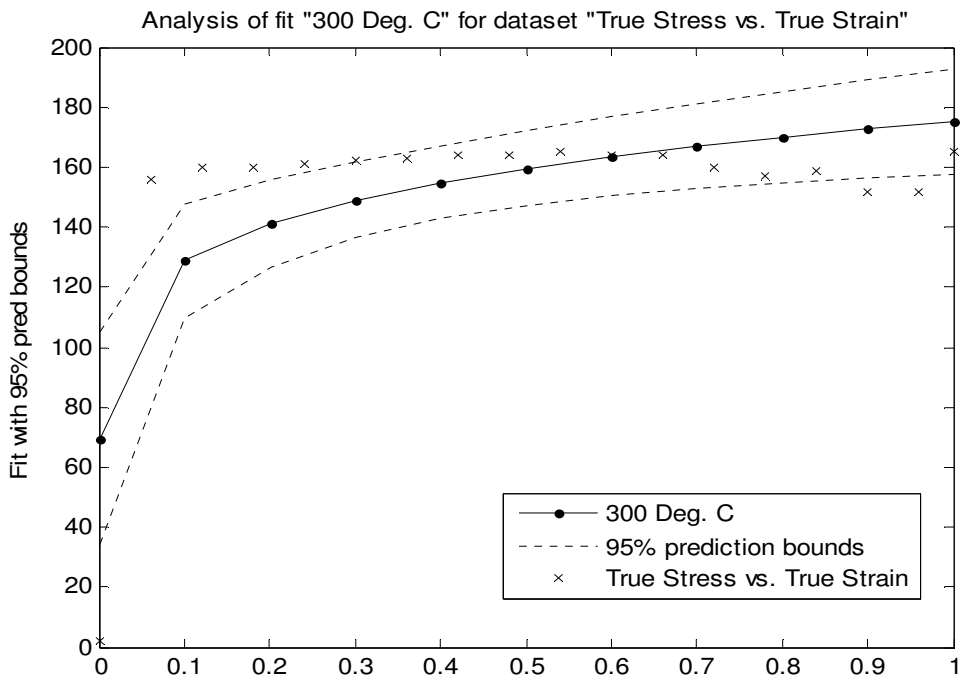

(f) Coefficients: $k = 175.1$, $n = 0.1339$

Figure 4. 1 Results Obtained From Regression Analysis

Non linear least square regression analysis gives a good fit to the experimental data as the R^2 values (Table 1) lying around 0.8. From the regression analysis the strength coefficient, *K* and strain hardening exponent, *n* for different temperature were obtained.

Table 4. 1 Results of Curve Fitting by Regression

Temperature(°C)	Goodness of Fit			
	SSE	R^2	Adj. R^2	RMSE
30	1.017e+004	0.8325	0.8220	25.21
100	8519	0.8364	0.8262	23.07
150	9491	0.8084	0.7964	24.26
200	8601	0.8008	0.7884	23.18
250	7363	0.7513	0.7358	21.45
300	9115	0.6211	0.5974	23.87

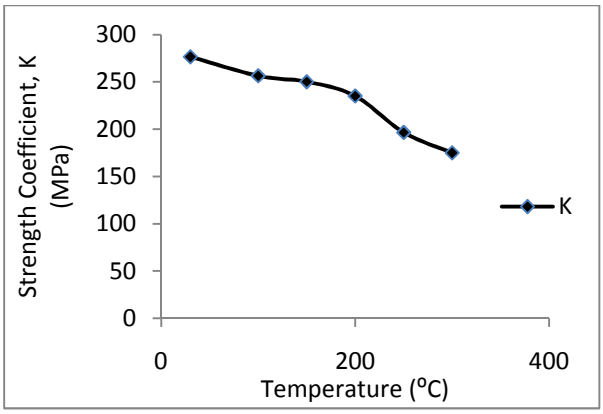

Figure 4. 2 Variation of K with Temperature

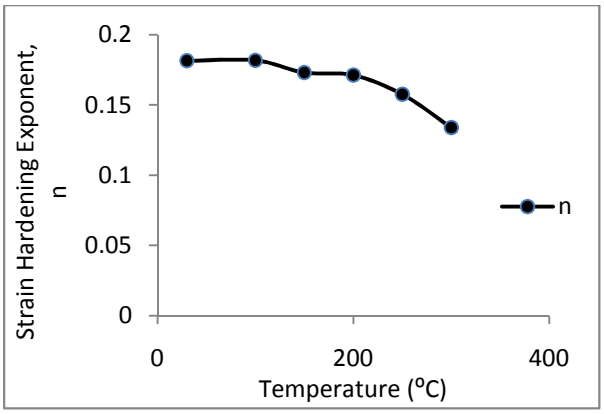

Figure 4. 3 Variation of n with Temperature

Figure 4.5 and 4.6 shows the variation of Strength Coefficient, *K* and Strain Hardening Exponent, *n* with the temperature respectively. Both the values decrease with the increase in temperature.

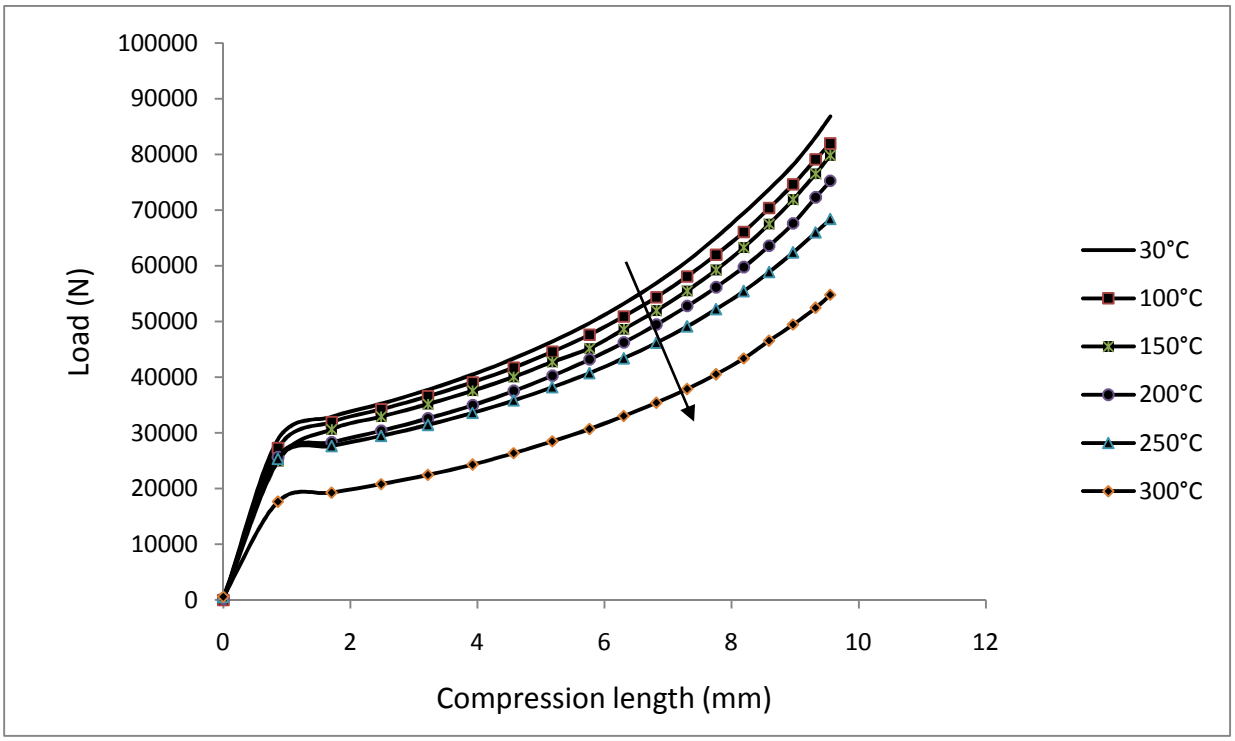

Figure 4. 4 Variation of load with Compression Length at Different Temperature for Strain of 1

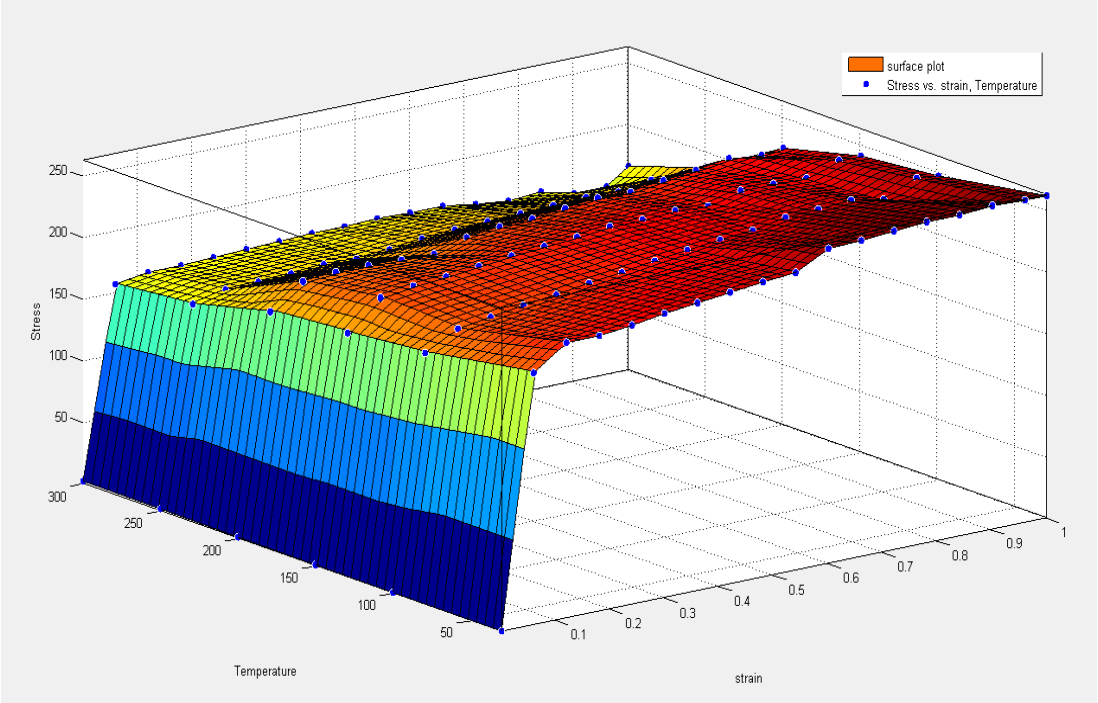

Figure 4. 5 Surface Plot of Stress vs. Strain and Temperature

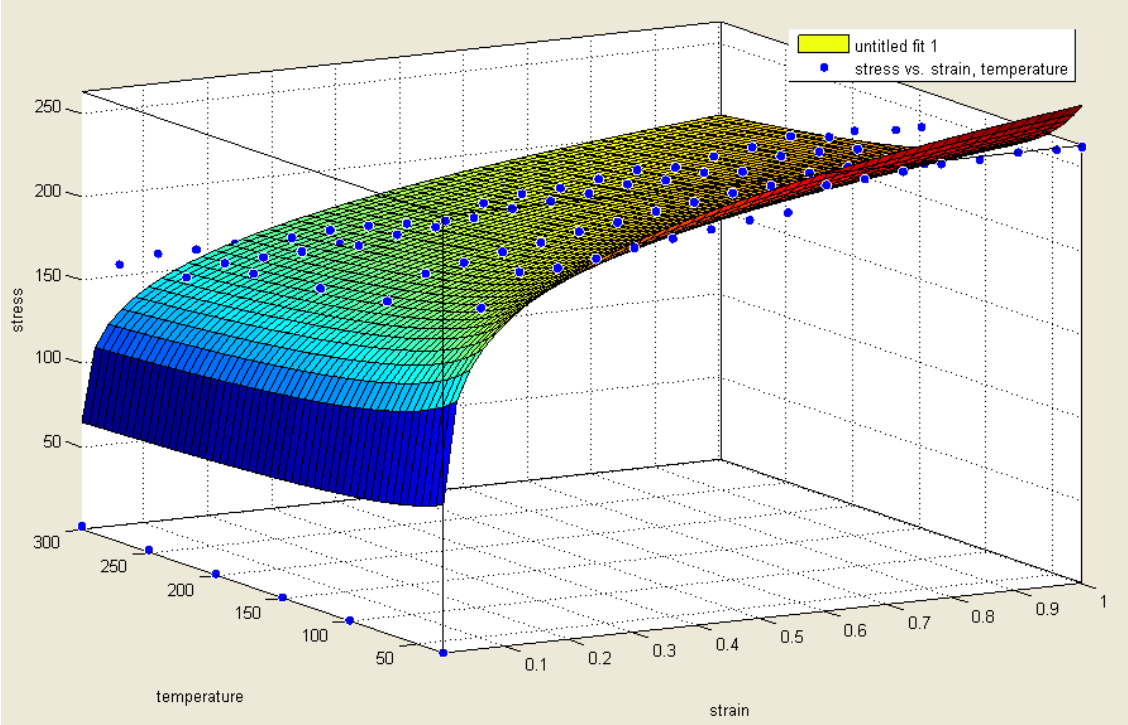

Figure 4. 6 Regression Plot for Fitting Surface Plot between Stress vs. Strain and Temperature

Non linear regression analysis results a common power equation considering both strain and temperature as follows

$$\sigma = A\varepsilon^m T^a \tag{3}$$

Where $A = 463.8, m = 0.1691, a = -0.1421$

Table 4. 2 Result of Regression for Common Fit

SSE	8.001e+004
R^2	0.763
Adj. R^2	0.7585
RSME	27.6

4.3 Radius of Curvature of the Barrel

The expression for the radius of curvature of the barrel [15] which follows a circular arc is as follows:

$$R = h_f^2/4(d_b - d_c) \tag{4}$$

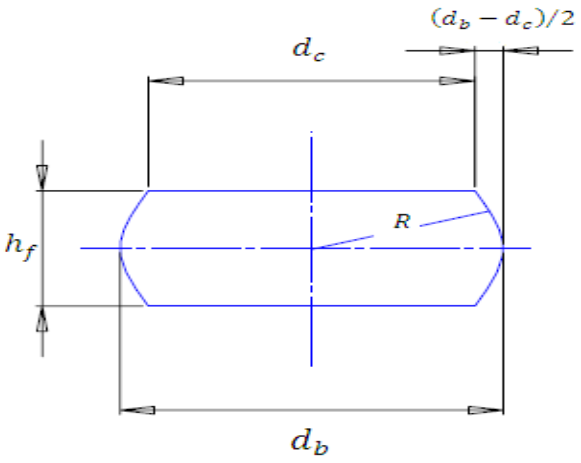

Figure 4. 7 Specimen Dimensions after Compression

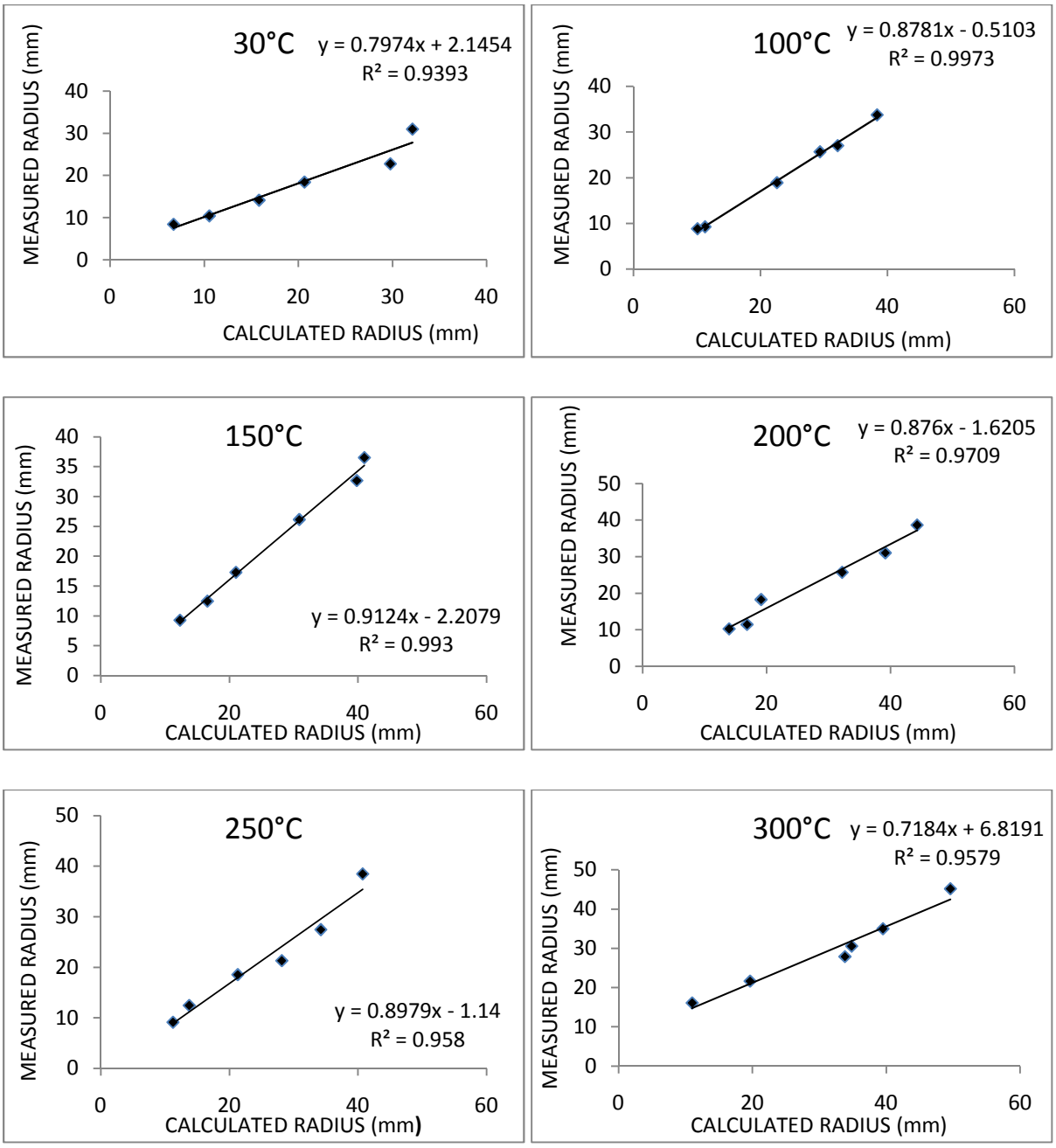

Figure 4. 8 Relationships between Measured Radius and Calculated Radius

Figure 4.10 shows that the calculated radius and measured radius of barrel bears a straight line relationship and both values are close to each other. So, taking the arc of barrel following a circular arc even at higher temperature is also justified.

Table 4. 3 Deviation of Calculated Radius from Measured Radius

Temperature (°C)	Strain	Measured R (mm)	Calculated R (mm)	Error (%)
30	0.5	30.98	32.13	3.71
	0.6	22.74	29.98	31.83
	0.7	18.4	20.65	12.22
	0.8	14.14	15.82	11.88
	0.9	10.42	10.53	1.05
	1	6.74	8.4	24.63
100	0.5	33.75	38.40	13.77
	0.6	27.02	32.17	19.06
	0.7	25.64	29.41	14.70
	0.8	18.9	22.62	19.68
	0.9	9.24	11.29	22.18
	1	8.82	10.10	14.51
150	0.5	36.51	41.01	12.32
	0.6	32.64	39.82	21.99
	0.7	26.12	30.88	18.22
	0.8	17.28	21.03	21.70
	0.9	12.43	16.58	33.34
	1	9.25	12.32	33.19
200	0.5	38.68	44.28	14.47
	0.6	31.04	39.15	26.18
	0.7	25.71	32.18	25.16
	0.8	18.24	19.12	4.82
	0.9	11.41	16.86	47.76
	1	10.21	13.95	36.63
250	0.5	38.45	40.73	5.93
	0.6	27.42	34.22	24.78
	0.7	21.29	28.14	32.17
	0.8	18.54	21.30	14.88
	0.9	12.45	13.75	10.44
	1	9.12	11.22	23.06
300	0.5	45.19	49.61	9.78
	0.6	34.97	39.51	12.98
	0.7	30.56	34.83	13.97
	0.8	27.88	33.84	21.37
	0.9	19.65	25.56	30.07
	1	10.98	16.06	46.26

4.4 Determination of Various Stresses

As explained elsewhere [15], the expression for bulging when following a circular arc, according to volume constancy principle for the barrel is as follows:

$$\frac{1}{4}\pi d_0^2 h_0 = \frac{1}{12}\pi(2d_b^2 + d_c^2)h_f \tag{5}$$

The above equation can be written as follows:

$$\frac{h_0}{h_f} = \frac{2d_b^2 + d_c^2}{3d_0^2} \tag{6}$$

Taking natural logarithm on both sides, the equation becomes:

$$\varepsilon_z = \varepsilon_\theta \tag{7}$$

Where: $\varepsilon_z = \ln\frac{h_0}{h_f}$ And $\varepsilon_\theta = \ln\left(\frac{2d_b^2+d_c^2}{3d_0^2}\right)$

Since the radial stress (σ_r) is zero at the free surface, it follows from the flow rule that:

$$\sigma_\theta = [(1 + 2\alpha)/(2 + \alpha)]\sigma_z \tag{8}$$

And that the effective stress can be expressed as:

$$\bar{\sigma} = (1/(2 + \alpha))\{3(1 + \alpha + \alpha^2)\}^{1/2}\sigma_z \tag{9}$$

The hydrostatic stress is given as follows:

$$\sigma_m = (1/3)(\sigma_\theta + \sigma_z) \tag{10}$$

where α is the slope between the hoop strain $(\varepsilon_\theta)$and the axial strain(ε_z)

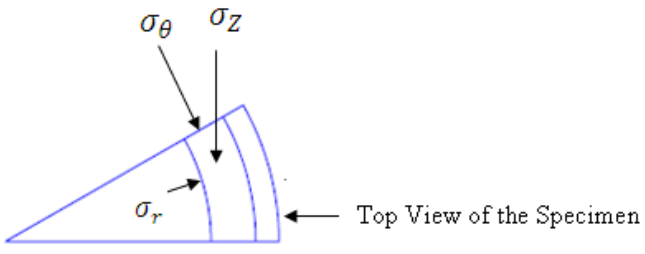

Figure 4. 9 Various Stresses Acting on the Specimen

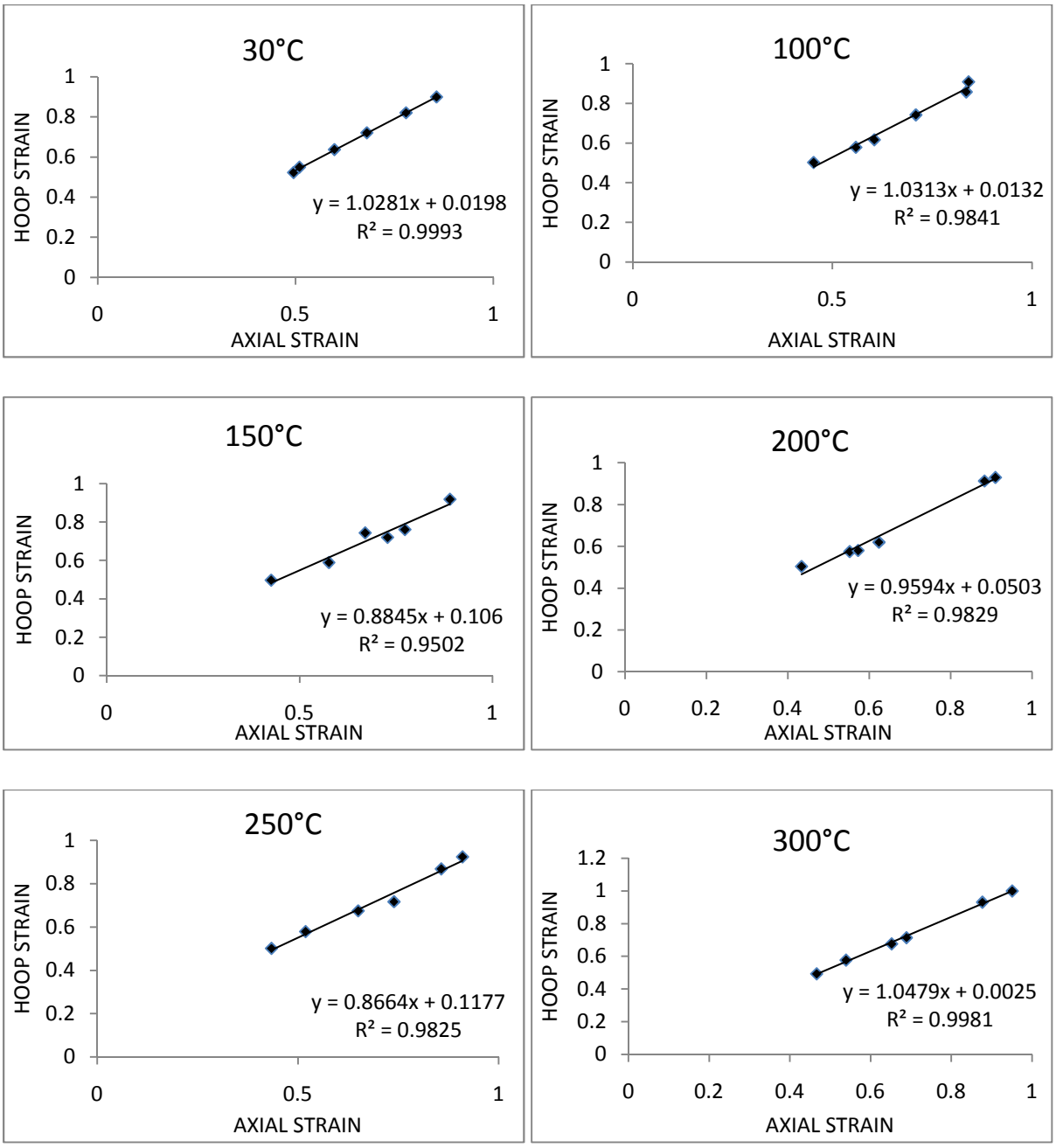

Figure 4. 10 Variation of Hoop Strain with Axial Strain

Figure 4.12 shows the relationship between hoop strain and axial strain. Slope of the relation ship gives the value of α. There was no regular relationship between α and temperature. The values of α were close to 1 as $\varepsilon_z = \varepsilon_\theta$ was considered for calculation purposes.

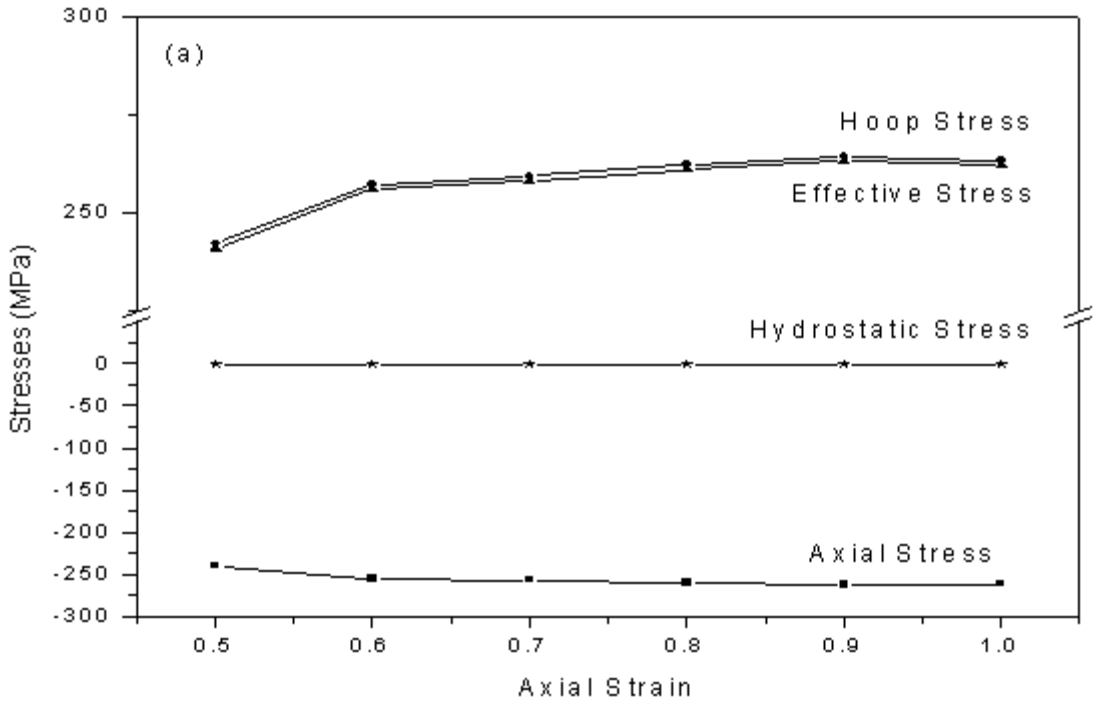
(a)
Hoop Stress
Effective Stress
Hydrostatic Stress
Axial Stress
Stresses (MPa)
Axial Strain
300
250
0
-50
-100
-150
-200
-250
-300
0.5
0.6
0.7
0.8
0.9
1.0

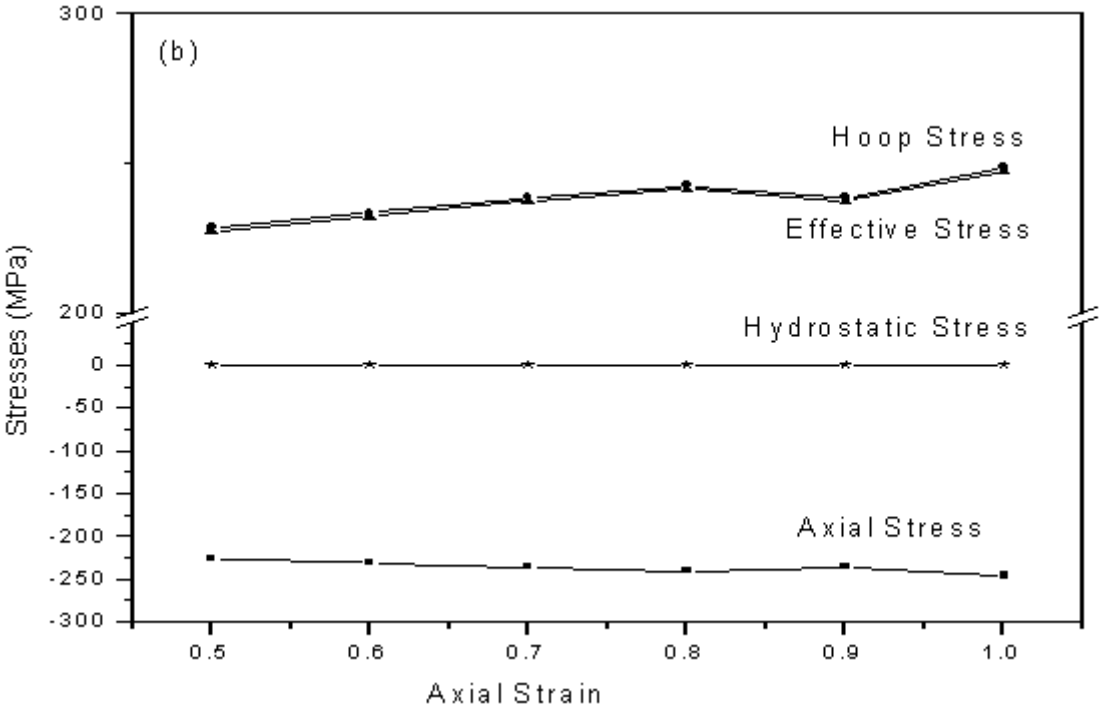
(b)
Hoop Stress
Effective Stress
Hydrostatic Stress
Axial Stress
Stresses (MPa)
Axial Strain
300
200
0
-50
-100
-150
-200
-250
-300
0.5
0.6
0.7
0.8
0.9
1.0

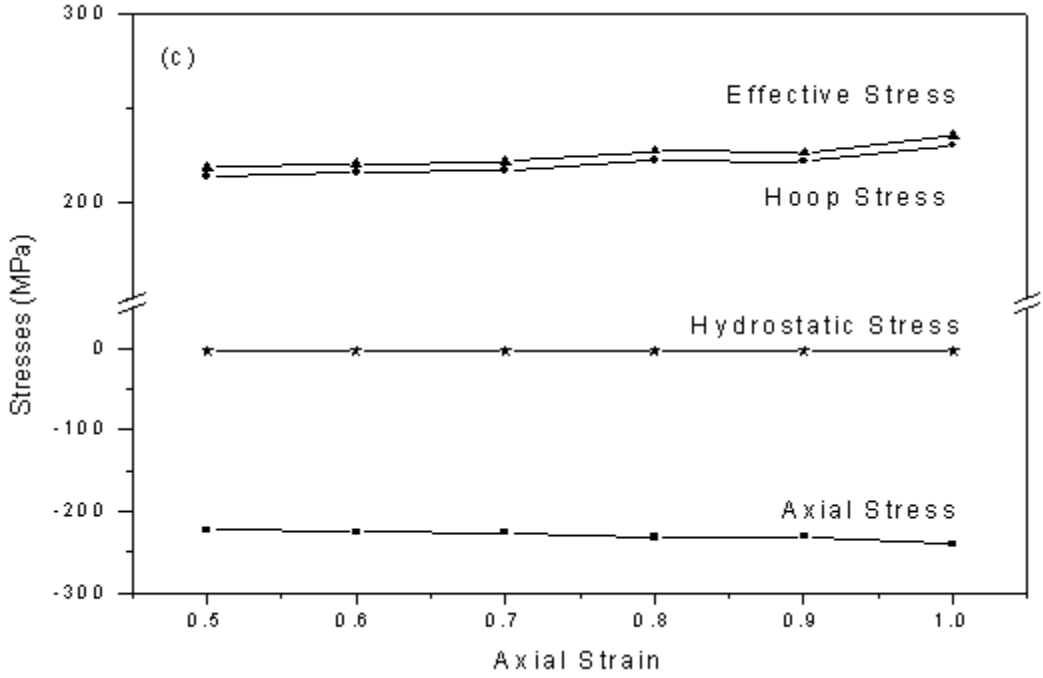
(c)
Effective Stress
Hoop Stress
Hydrostatic Stress
Axial Stress
Stresses (MPa)
300
200
0
-100
-200
-300
0.5
0.6
0.7
0.8
0.9
1.0
Axial Strain

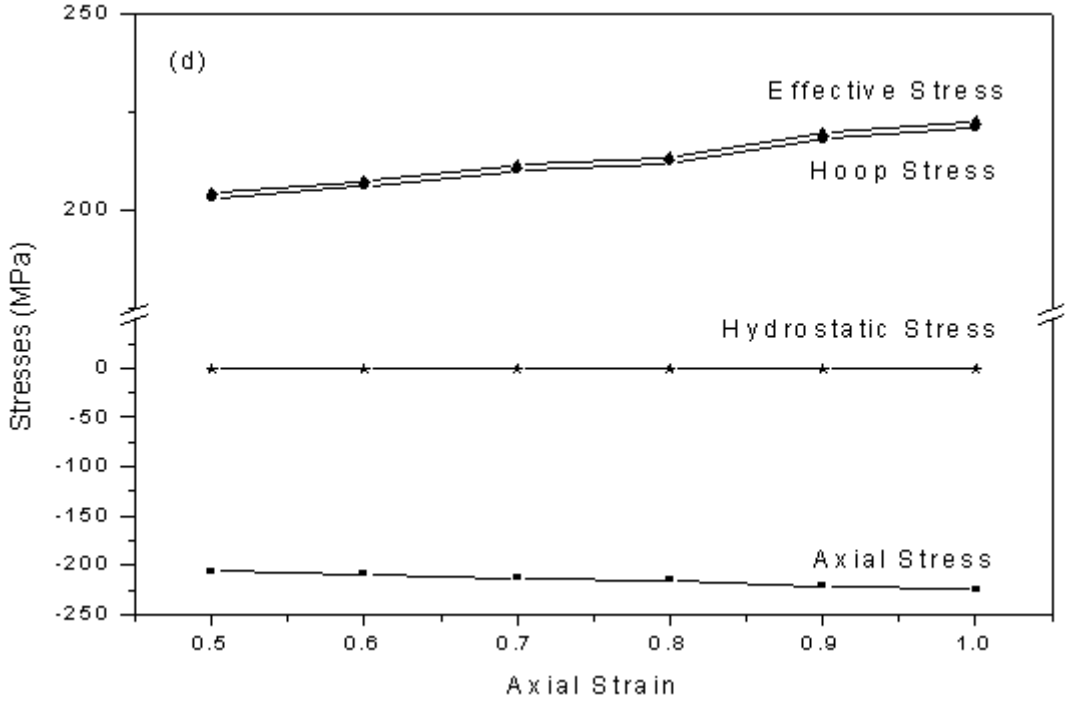
(d)
Effective Stress
Hoop Stress
Hydrostatic Stress
Axial Stress
Stresses (MPa)
250
200
0
-50
-100
-150
-200
-250
0.5
0.6
0.7
0.8
0.9
1.0
Axial Strain

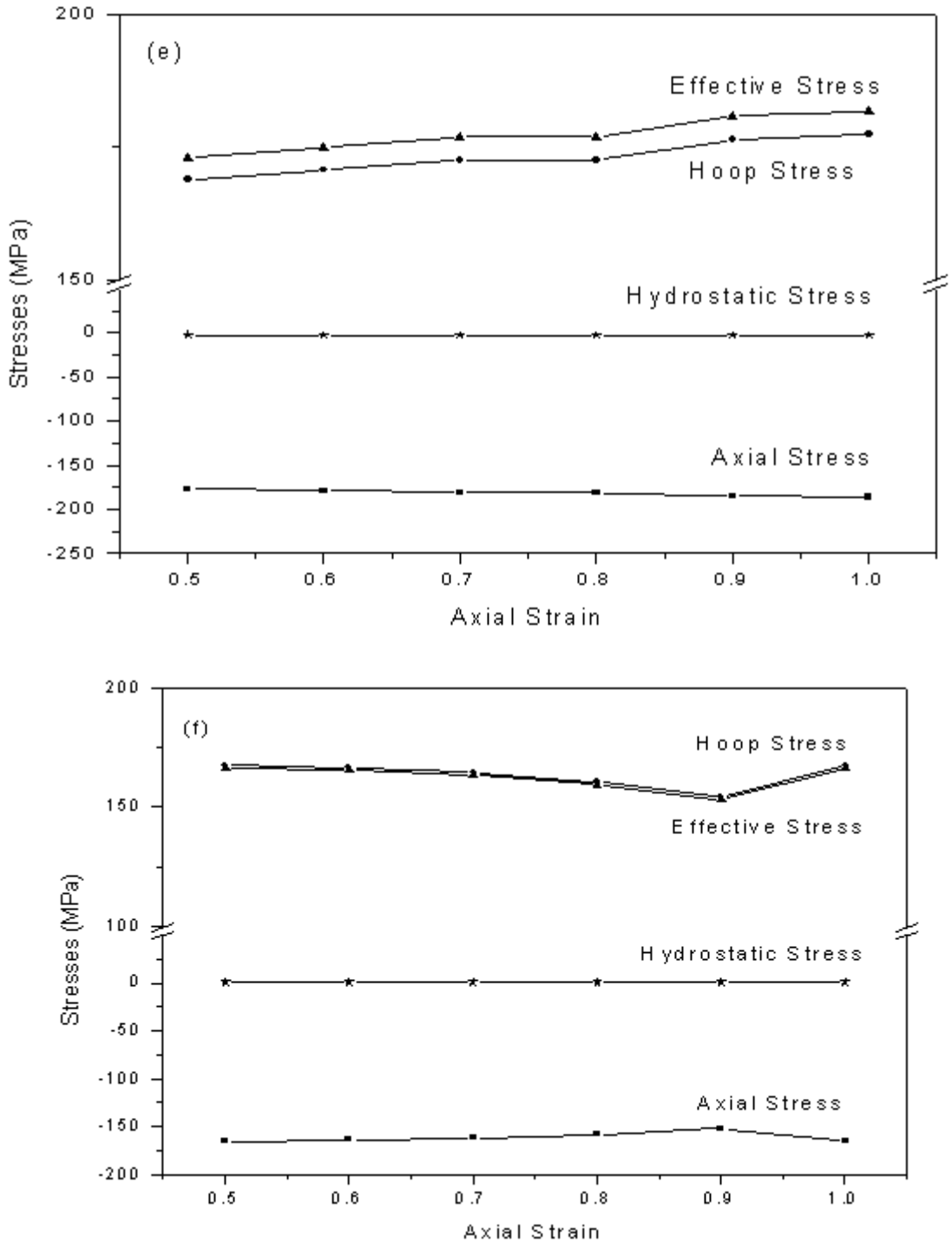

Figure 4. 11 Variation of Different Stress for Different Temperature, (a)-(f): 30°C-300°C

Figure 4.13 shows the various stresses acting on the specimen during the experiment at different temperature. The axial stress is negative as it is compressive in nature where as effective stress

and hoop stress were positive as they were tensile in nature and the nature of the hydrostatic stresses depends on the values of α.

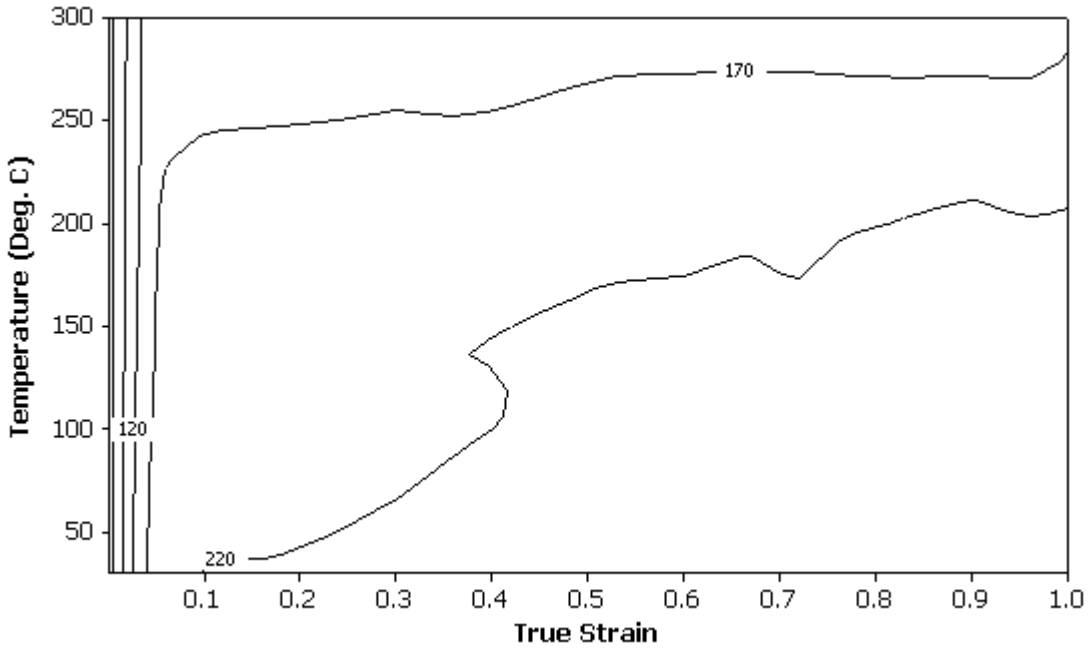

Figure 4.12 Contour Plot

Figure 4.14 shows the contour plot which shows the effect of temperature and strain on true stress.

Chapter 5
Conclusions

5. Conclusions

Following conclusions were made from the above work:

(1) Flow stress, Strain hardening exponent *n* and strength coefficient *K* all decreases with the increase in temperature. Consideration of taking barrel shape following as a circular arc also holds good at elevated temperature.

(2) The calculated and measured radius of curvature of barrel was close to each other. The radius value increases with the increase in test temperature and decreases with the increases in amount of strain.

(3) The value of different stresses depends on the slope (α) of the hoop strain and axial strain. Nature of the hydrostatic stress changes from compressive to tensile depending on α.

References

[1] Jin Nengping. et. al Hot deformation behavior of 7150 aluminum alloy during compression at elevated temperature, Journal of Materials characterization 60 (2009)530-536.

[2] Poursina.M. et.al Flow stress behavior of two stainless steels: An experimental-numerical investigation, Journal of materials processing technology 199 (2008) 287-294.

[3] Zhang Hui et.al, Hot deformation behavior of the new Al-Mg-Si-Cu aluminum alloy during compression at elevated temperatures, Journal of Materials characterization58 (2007) 168-173.

[4] Xiu-yu WEI. et.al, Flow stress of 2197 Al-Li alloy during hot compression deformation, Transaction of non ferrous metals society of China 17 (2007) s280-s284.

[5] Cerri.E. et.al, Hot compression behavior of the AZ91 magnesium alloy produced by high pressure die casting, Journal of Materials Processing Technology 189 (2007) 97–106.

[6] Zhu. Su-Ming. et.al, A comparative study of the high temperature deformation behavior of Fe-25Al and Fe-25Al-10Ti alloys, Journal of Scripta materialia 42 (2000) 905–910.

[7] Zhang.X.Y.et.al, Deformation behavior in isothermal compression of the TC11 titanium alloy, Materials and Design 31 (2010) 2851–2857.

[8] Herrmann. J. et.al, Deformation behavior of iron-rich iron-aluminum alloys at high temperatures, Acta Materialia 51 (2003) 3233–3242.

[9] Talebi Anaraki. M. et.al, Modeling of high temperature rheological behavior of AZ61 Mg-alloy using inverse method and ANN, Materials and Design 29 (2008) 1701–1706.

[10] Mousavi Anijadan. S.H. et.al. Flow Stress Optimization for 304 Stainless Steel under Cold and Warm Compression by Artificial Neural Network and Genetic Algorithm, Materials and Design 28 (2007) 609-615.

[11] Aluko. O. et.al, Warm Compression Tests of Aluminum Alloy, Journal of Materials Engineering and Performance 7 (1998) 474-478.

[12] Mandal S. et. al. Constitutive equations to predict high temperature flow stress in a Ti-modified austenitic stainless steel, Journal of Materials science and engineering A 500 (2009) 114-121.

[13] Chen. Z.Y. et.al. Deformation Behavior of Aa6063 Aluminium Alloy After Removing Friction Effect under Hot Working Conditions, Acta Metall. Sin. (Engl. Lett.) Vol.21 No.6 (2008) 451-458.

[14] Ramanathan. S. et.al. Hot Deformation Behavior of 2124 Al Alloy, Journal of Material Science Technology, Vol.22 No.5, (2006) 611-615.

[15] Narayansamy. R. et.al, Phenomenon of Barreling in Aluminum Solid Cylinders during Cold Upset Forming, Journal Of Materials Processing Technology 70 (1997) 17-21.

[16] Narayansamy. R. et.al, A Study on Barreling in Magnesium Alloy Solid Cylinders during Cold Upset Forming, Journal of Materials Processing Technology 101 (2000) 64-69.

[17] Manisankar. K. et. al, Phenomenon of Barreling in Square Billets of Aluminum Alloy during Cold Upset Forming, International Journal of Advance Manufacturing Technology 21 (2003) 84-49.

[18] Malayappan. S. et. al, Some Aspects on Barreling in Aluminum Solid Cylinders During Cold Upset Forging using A Die with Constraints, Journal of Materials Processing Technology 135 (2003) 18-29.

[19] Manisankar. K. et. al, Effect of Friction on Barreling in Square Billets of Aluminum during Cold Upset Forging, Journal Of Materials And Design 27 (2006) 147-155.

[20] Malayappan. S. et. al, Barreling of Aluminum Solid Cylinders during Cold Upsetting with Differential Frictional Conditions at the Faces, International Journal of Advance Manufacturing Technology 29 (2006) 41–48.

[21] Sljapic. V. et.al, Observations on Fracture in Axi-Symmetric and Three-Dimensional Cold Upsetting of Brass, Journal of Materials Processing Technology 125-126 (2002) 267-274.

[22] Dieter George E., Mechanical Metallurgy. London, McGraw-Hill Book Company, 2005.

[23] Kalpakjian S. and Schmid. S. R., Manufacturing Engineering and Technology, Dorling Kindersley (India) Pvt. Ltd., Pearson Education, 2009.

[24] http://www.instron.us/wa/home/default_en.aspx